Realizing 20% External Quantum Efficiency in Electroluminescence with Efficient Thermally Activated Delayed Fluorescence from an Exciplex

Marian Chapran,[§1] Piotr Pander,[§2] Marharyta Vasylieva,[3] Gabriela Wiosna-Salyga,[1] Jacek Ulanski,[1] Fernando B. Dias [2]* and Przemyslaw Data [2,3,4]**

[1] Lodz University of Technology, Department of Molecular Physics, Zeromskiego 116, 90-924 Lodz, Poland

[2] Physics Department, Durham University, South Road, Durham, DH1 3LE, United Kingdom

[3] Faculty of Chemistry, Silesian University of Technology, M. Strzody 9, 44-100, Gliwice, Poland

[4] Centre of Polymer and Carbon Materials, Polish Academy of Science, M. Curie-Sklodowskiej 34, 41-819, Zabrze, Poland

KEYWORDS: exciplex, thermally activated delayed fluorescence, TADF, OLED

ABSTRACT: The investigation of non-doped exciplex blends of 2,4,6-Tris[3-(diphenylphosphinyl)phenyl]-1,3,5-triazine (PO-T2T), working as the one-electron acceptor molecule, with different electron donors is reported. The emissions of these exciplexes span from the blue to orange-red regions, showing clear contribution from thermally activated delayed fluorescence (TADF) and delayed fluorescence originated from non-geminate recombination of charge carriers created by the dissociation of optically generated exciplexes. We focus our

studies on the properties of TADF in these systems, covering in particular the physical meaning of the different transient components observed in their luminescence decays. Our results unravel the intricate role of reverse intersystem crossing due to spin-orbit coupling and possibly also due to hyperfine interactions and internal conversion, which affect the efficiency of the TADF mechanism. Remarkable performances are obtained in prototype organic light-emitting diodes fabricated with some of these blends. Green exciplex blends, in particular, exhibited the current efficiency of 60 cd A^{-1}, power efficiency of 71 lm W^{-1} and external quantum efficiency of 20%. We believe our results will contribute significantly to highlight the potential advantages of intermolecular exciplexes in the area of organic light-emitting diodes.

INTRODUCTION

The development of organic light-emitting diodes (OLEDs) and their application in solid-state lighting (SSL) and display technologies is followed with great interest by researchers and industry. One of the classical approaches to obtain multi-colour OLEDs is based on using guest-host systems, where blue, green and red thermally activated delayed fluorescence (TADF) emitters are doped in suitable hosts.[1,2] However, this approach creates important technical challenges, including the choice of appropriate host materials for the different TADF molecules ("host tuning"),[3] and the need to optimize the concentration of the guest in the host, which makes the realization and control of OLEDs very challenging.

Exciplex states were introduced to the OLED arena many years ago due to the work of various researchers, including the groups of Kalinowski and Adachi.[4–7] However, in general, “single” TADF molecules show higher performance in OLEDs, when compared with bimolecular exciplexes. This is mainly due to the low photoluminescence quantum yield (Φ_{PL}) of exciplexes,

but also due to the favorable molecular orientation of the TADF molecules that can engineered to maximize the intrinsic low light outcoupling efficiency associated with emitting organic layers, [8–10] but it is difficult to control in the case of bimolecular systems. The relatively weak luminescence of exciplex blends follows well known opposite trend between the charge transfer (CT) character and PLQY due to the weak electronic coupling of the excited state with the ground state of strong charge transfer molecules. This fact has limited the use of exciplexes to fabricate efficient devices, and is especially true in the red region where enhanced internal conversion contributes to quench the triplet population due to the energy-gap law.[11,12] The blue region [13] is also difficult for the bimolecular exciplexes as they tend to form more stabilized CT states and emission in the green region. To the best of our knowledge no efficient red exciplex has been reported to date, which represents a serious problem for the possible application of exciplex blends in white OLEDs. Moreover, the broad Gaussian-type emission spectra of exciplex systems does not provide good color purity and does not satisfy the National Television System Committee (NTSC) requirements, which creates additional problems to explore these systems in displays. However, exciplexes offer a very interesting alternative approach to realize multi-color OLEDs employing one acceptor and several different donors to simultaneously achieve multi-color luminescence and efficient triplet harvesting. Exciplex also offer a promising alternative to intramolecular TADF molecules, giving the possibility to fabricate OLEDs without using a host material, i.e. the emitting layer in OLEDs using exciplex working cumulatively as the emitter and the host, which will bring significant savings in production costs. Therefore, discovering ways to maximize the luminescence efficiency in exciplexes, while keeping strong triplet harvesting, is key for their implementation in the OLED field and important for both intramolecular and intermolecular systems.

A significant breakthrough in exciplex emitters was achieved when the thermally activated delayed fluorescence (TADF) properties of several exciplexes, including the m-MTDATA:PBD system,[4] was discovered by Adachi and co-workers. This idea was later explored by other research groups[15–22] who showed that very efficient triplet harvesting can be achieved in exciplex systems.

The development of novel exciplex emitters should, therefore, focus on achieving high luminescence efficiencies, while efficient triplet harvesting (TADF) is maintained, so bimolecular systems can compete with their "single" molecule counterparts. This task is complex and requires deep understanding of the photophysics of exciplex blends to unravel the more elusive aspects of the mechanism that affect the luminescence efficiency and lifetime of in different regions of the spectrum. Despite TADF exciplexes have already been used as efficient OLED emitters, they remain in some ways an unsolved puzzle for photophysicists. Some aspects of the theory that is used to explain the formation and decay of these intermolecular excited states are relatively simple, however, their use in practical systems, such as OLEDs, reveal that intermolecular TADF exciplexes are clearly more complex than their intramolecular analogues. For example, the luminescence decay of exciplexes shows prompt and delayed fluorescence components, which are also present on the luminescence decay of TADF molecules, however, more often in the exciplexes than in the "single" TADF emitters the luminescence decay includes a luminescence component decaying in a power law fashion, usually observed in the μs to ms region.[23] The origin of these power-law decays is still not clear, but certainly involves long-lived recombination processes. Therefore, the design of more efficient exciplexes, with shorter luminescence lifetimes, requires the understanding of the physical reasons behind power law regimes, so the luminescence quenching due to charge carriers can be minimized in devices.

Importantly, recent works showed that some theories that apply to molecules that form intramolecular CT states can be also applied to intermolecular exciplexes, giving grounds to treat mono- and bimolecular CT emitters alike.[24]

Here we discuss the photophysics of a carefully selected set of intermolecular exciplex blends with emission in the blue to orange regions of the visible spectrum. Our motivation is to obtain a clear picture of the photophysical processes that affect the luminescence efficiency of these blends in different regions of the visible spectrum. The photophysics is also correlated with device data. Remarkably, devices with external quantum efficiencies (EQE) up to 20% were achieved in some of these blends, demonstrating the usefulness of exciplexes as OLED emitters, and underlining their major advantages over intramolecular TADF emitters. This includes the easy color tuning of their emission, and the fact that efficient TADF exciplex systems may be, at least theoretically, produced using already existing molecules, which are often reported in the literature or are even commercially available. This study brings also clear physical meaning to the transient components observed in the luminescence decays of exciplexes, explaining the observation of luminescence regimes decaying as a power law in many exciplex emitters. Finally, the photophysical observations are correlated with the efficiencies of exciplex systems under electrical excitation (and electrical field), using the D:A pairs implemented in multi-colour OLEDs. These findings will facilitate the design of more efficient exciplex systems in the future.

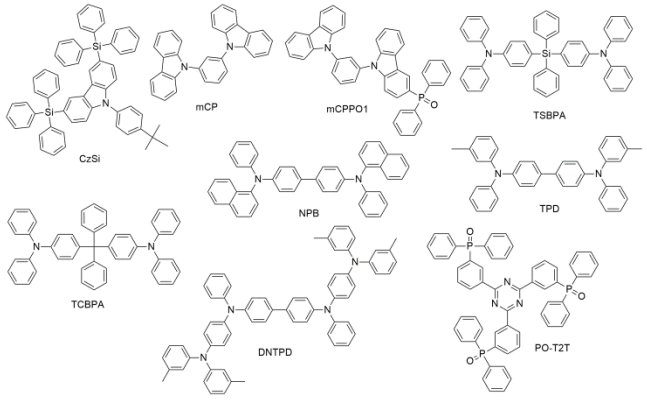

Figure 1. Chemical structures of materials used in this work.

RESULTS AND DISCUSSION

Exciplexes can be formed between electron donating (D) and electron-accepting (A) molecules, where the highest occupied molecular orbital (HOMO) is distributed on the D molecule and the lowest unoccupied molecular orbital (LUMO) is located on the A molecule.[4,25,26] The excited state complex is created with extremely small energy difference between singlet and triplet states (ΔE_{ST}) due to the negligible overlap between HOMO and LUMO. This contributes to very efficient triplet harvesting in OLEDs. **Figure 1** shows the chemical structures of the compounds studied in this work. Most of these molecules are currently used as hole (TSBPA, TCBPA, NPD, TPD, DNTPD) or electron (PO-T2T) transport layers, or used as blocking layers (TSBPA, TCBPA), or even as hosts (CzSi, mCP, mCPPO1) in OLEDs. To the best of our knowledge, exciplex blends formed with these molecules have never been reported (except for mCP:PO-T2T[27,16] and NPB:PO-T2T[28]). PO-T2T was chosen as the acceptor due to its high electron affinity (3.14 eV), high electron mobility ($1.7\text{-}4.4\times10^{-3}$ cm^2 $V^{-1}s^{-1}$),[29] and high triplet energy (2.93 eV).

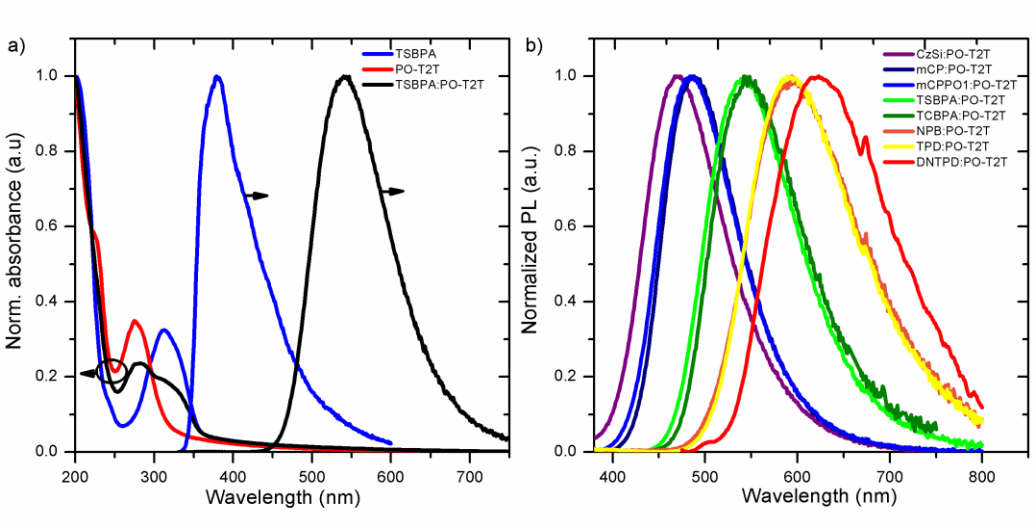

Figure 2. a) Normalized absorption spectra of TSBPA, PO-T2T and their blends in pristine films, b) photoluminescence spectra of all exciplexes obtained in solid films in air.

Steady-state spectroscopy. Figure 2a shows the absorption and steady-state fluorescence spectra of the individual TSBPA donor and PO-T2T acceptor molecules, as well as their exciplex-forming blend as an exemplar of the exciplex properties of these blends. The absorption spectrum of the blend is simply a superposition of the absorption of the donor and acceptor absorptions, and there is no evidence of formation of CT complexes in the ground state. Similar observations were made for other blends (**Figure S1**). **Figure 2b** shows the photoluminescence (PL) spectra of all exciplex blends studied in this work. It is particularly noteworthy that all presented blends show exciplex-only emission, with broad, Gaussian shape, typical of CT state emission,[30] clearly red shifted in respect to the emission of their individual D and A constituents, as evidenced in **Figure S2**. Moreover, as shown in **Figure 3** the ^{1}CT energy is a function of IP_D-EA_A energy difference, similarly to other reported exciplexes[25,31,32] (**Table 1, Table S5**).

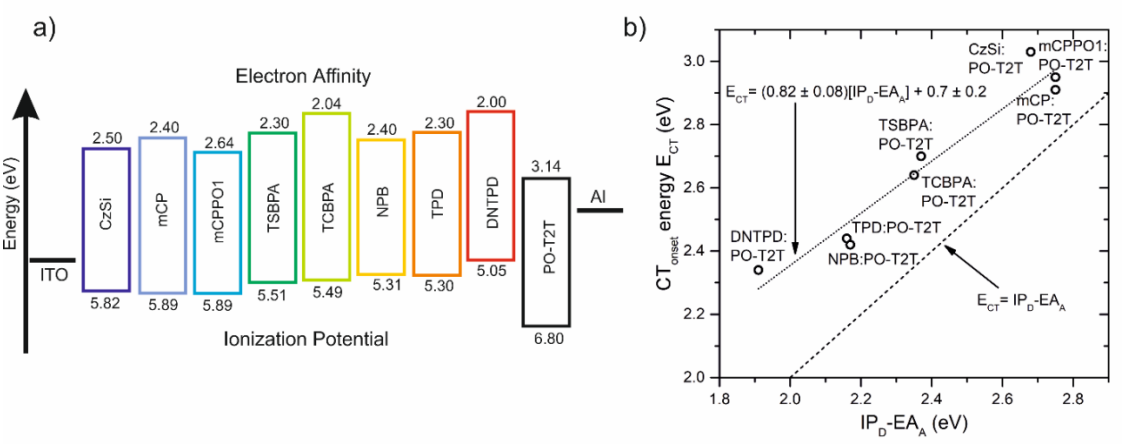

Figure 3. a) Energy levels of investigated donors and acceptors; b) *onset* CT energy plotted against electrochemically derived IP_D-EA_A energy difference.

TADF in exciplexes and the role of local triplet states (^{3}LE). As in exciplex systems the overlap between the HOMO and LUMO orbitals of the D and A units, respectively, is minimal, the energy of the exciplex singlet state (^{1}CT), determined from the onset of the exciplex fluorescence, and the energy of the triplet state (^{3}CT) can be assumed as nearly identical. However, very often the triplet state with lower energy in the system is of local character, i.e. it is localized on the donor (D) or acceptor (A) molecules, and end up controlling the S-T energy gap in the exciplex system. Therefore, while the CT state energy is a function of donor and acceptor HOMO-LUMO levels, and thus can be tuned, the energy of the local triplet state is determined by the triplet energy of either the donor or the acceptor molecules.[24,33] This implies that each donor-acceptor pair may have different relative energy alignment of the CT state in relation to the local triplet state(s) (^{3}LE), which is in part controlled by the large stabilization of the CT states, as it is evident from the large Stokes-shift of the exciplex luminescence. This situation leads to one of three cases that have been used to describe the TADF mechanism in exciplexes:[34,35] (**I**) The ^{3}LE lies visibly below the ^{1}CT state, such as in the exciplexes described

in previous works;[24] (**II**) The energy of the ^{3}LE state is aligned with the ^{1}CT state, such as in mCP:PO-T2T or mCPPO1:PO-T2T exciplexes; (**III**) The ^{3}LE is clearly above the ^{1}CT state, such as in TSBPA:PO-T2T or TCBPA:PO-T2T. Case (**II**) is the ideal situation for efficient reverse intersystem crossing (RISC) to occur. Here, the ^{3}LE state has an intermediating role between the ^{1}CT and ^{3}CT states and enables fast RISC due to spin-orbit coupling interaction involving the ^{1}CT/^{3}CT and the ^{3}LE states.[33] In contrast, the lower-lying ^{3}LE state in case (**I**) creates an energy barrier between ^{1}CT and ^{3}LE, which may even be too large for TADF to occur at room temperature. In case (**III**), because ISC and RISC between ^{1}CT and ^{3}CT due to spin-orbit coupling is formally forbidden by symmetry, RISC is expected to be less favorable.[33,36–38] This, assuming that the hyperfine coupling between ^{1}CT and ^{3}CT states cannot provide fast exchange.[33–37,39] Therefore, the only way to convert triplet states from ^{3}CT to ^{1}CT involves the electronic coupling with the ^{3}LE state, which again generates an energy barrier for TADF. Surprisingly, our results show that for TSBPA:PO-T2T and TCBPA:PO-T2T exciplexes efficient RISC occurs even when the ^{3}LE states are well above the ^{1}CT state, by 0.20 and 0.32 eV, respectively. Moreover, efficient TADF and high OLED EQE is achieved for both TSBPA:PO-T2T and TCBPA:PO-T2T blends. We will address the exciplex TADF mechanism to explain these results later in this work.

Table 1. Electronic and photophysical properties of investigated exciplexes.

Exciplex	IP_D-EA_A, eV[a]	CT_{relax}, eV[b]	^3LE_D, eV[c]	^3LE_A, eV[d]	ΔE_{ST}, eV[e]	τ_{PF}, ns[f]	τ_{DF}, μs[g]	DF/PF ratio[h]
CzSi:PO-T2T	2.68	3.03	3.05	2.93	0.10	36 ± 3	6.3 ± 0.3	5.7
mCP:PO-T2T	2.75	2.91	2.90		≈ 0.01	16 ± 1	1.96 ± 0.07	4.2
mCPPO1:PO-	2.75	2.95	2.96		≈ 0.02	17 ± 3	2.63 ±	7.3

T2T							0.15	
TSBPA:PO-T2T	2.37	2.70	2.90		≈ 0*	30 ± 6	2.2 ± 0.2	15.1
TCBPA:PO-T2T	2.35	2.64	2.96		≈ 0*	27 ± 6	2.2 ± 0.2	14.9
NPB:PO-T2T	2.17	2.42	2.44		≈ 0*	21 ± 2	0.53 ± 0.04	1.0
TPD:PO-T2T	2.16	2.44	2.45		≈ 0*	19 ± 1	0.37 ± 0.02	2.3
DNTPD:PO-T2T	1.91	2.34	2.43		≈ 0*	12 ± 1	-	-

[a] ionization potential of the donor (IP_D) – electron affinity of the acceptor (EA_A) difference; [b] energy of the relaxed CT emission recorded from delayed fluorescence spectra; note the energy recorded for DNTPD:PO-T2T exciplex, due to lack of TADF, is for prompt fluorescence emission; [c] triplet energy of the donor; [d] triplet energy of the acceptor; [e] singlet-triplet energy splitting; [f] prompt fluorescence lifetime; [g] delayed fluorescence lifetime; [h] delayed fluorescence to prompt fluorescence ratio derived as a ratio of integrated delayed fluorescence (DF) and prompt fluorescence (PF) intensity from the fitted decay curves. * $^1CT - ^3CT$ approaches 0 eV.

As already mentioned, exciplexes usually show low photoluminescence yield (Φ_{PL}). This is direct consequence of a truly distinct HOMO and LUMO orbitals showing vanishingly small overlap. Small, nearly zero integral overlap causes the transition oscillator strength to be very low,[40] with direct impact on the radiative rate of the excited state. This is in fact also a problem in many D-A TADF emitters, and it is believed that in order to obtain good oscillator strength in an exciplex the D and A species must be very close to each other. The PLQY of TADF molecules in general are obviously affected by the radiative rate constant as in any other molecules. However, particular for the TADF case is the fact that triplets can also contribute to the PLQY. Therefore, the competition between the RISC rate and the non-radiative rate that affect the triplet decay have to be taken into consideration. For example, let's consider a system where the RISC rate dominates over the non-radiative decay in the triplet state. In this scenario,

any triplet will be up-converted to the singlet manifold, from where it can emit or return back to the triplet state, due to ISC, however as the RISC dominates, once it arrives in the triplet state it will return back to the singlet state, from where it has one more chance to emit. This is known as the recycling process in TADFs. As the PLQY takes into account both prompt and delayed fluorescence components, it can be high even if the radiative rate is relatively slow. The crucial occurrence is that the internal conversion needs to suppressed. Obviously a larger radiative rate will also help. Given the high ΦPL of the TSBPA and TCBPA blends with PO-T2T, we therefore, speculate that the PO-T2T star-shaped molecule with relatively planar structure should make it easier to minimize the non-radiative internal conversion in these systems. Probably, it may also that the D and A molecules in these blends are closer to each other, allowing for relatively large orbital overlap and thus increasing the radiative rate in TSBPA and TCBPA blends with PO-T2T. [41]

Explaining the photoluminescence decay components observed from exciplex blends using time-resolved spectroscopy. In all photoluminescence decays of the presented exciplex blends there are three clear decay regions, however, this is more evident in some of the cases (**Figure 4**). Interestingly, these regions can all be fitted using simple decay laws. Two of these regions can be described using single exponential expressions, these are the short-lived prompt fluorescence and the long-lived TADF region, whereas a third region can only be fitted using a power law decay.[23] It is well known that exponential expressions are able to adequately describe the decay of singlet and triplet populations of "well-behaved" exciplexes, i.e. those that have a very narrow distribution of decay lifetimes. In brief an exponential decay occurs when there is a single species emitting at constant rate. This is often the case in solution. However, in films, power-law decay laws are often needed to describe the luminescence decays. In principle this

can be interpreted as due to the presence in the blend of a broad distribution of decay lifetimes originated by the geometry and distance heterogeneity among the exciplex constituents in the blend. However, it immediately becomes evident that the appearance of power law decays may be in fact caused by a completely different phenomenon.

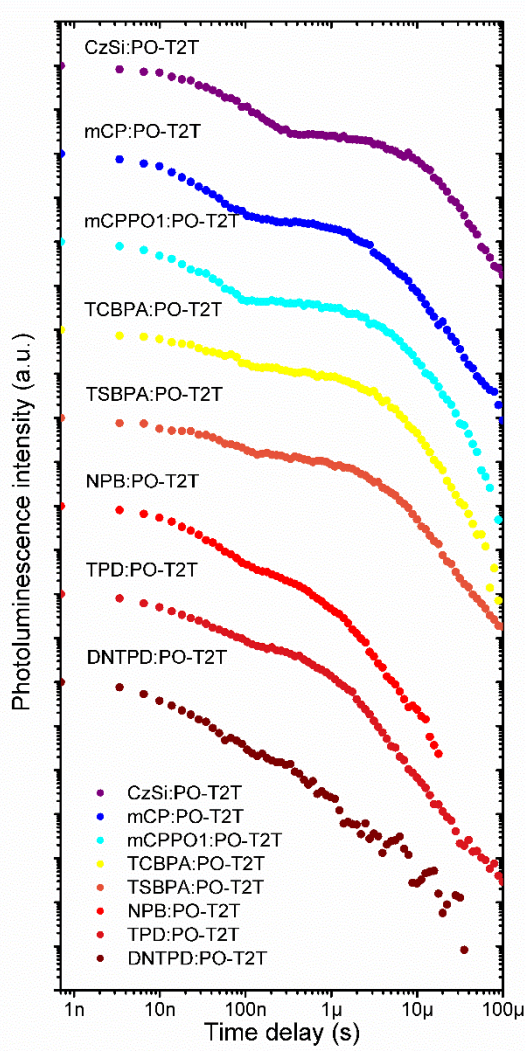

Figure 4. Room temperature photoluminescence decay of investigated exciplex blends (λ_{exc} = 355 nm). Note all exciplexes are formed with respective donor and PO-T2T as an acceptor. Note: donor-acceptor ratio is 1:1. Decays recorded in a vacuum at 295 K.

In the light of a recent paper by Kabe and Adachi,[42] it may be that in some situations the exciplex state may dissociate into a separate hole and an electron. This pathway cannot be neglected when describing the recombination of charge carriers in solid films. The explanation given by the authors on the behavior of their exciplex system appears consistent with the power law decay reported in this work.[42] Both singlet and triplet exciplex states may dissociate into freely separated hole an electron, which are able to migrate, via hopping, through donor- or acceptor-dominated domains, respectively. These charges when recombining at later time give origin to singlet and triplet exciplex states, which produce delayed exciplex fluorescence (**Figure 5**). As their migration pathways vary in a broad range, their recombination lifetime shows a broad distribution, which can only be fitted by a power law decay (**Figure 4, 6a**). This observation is further supported by a recently published study[43] presenting experimental evidence for formation of polaron pairs in exciplex blends upon light illumination. In this more recent report, the authors suggest the polaron pairs remain a non-radiative evolution pathway of the exciplex state. This is contrary to the explanations suggested by Kabe and Adachi[42] and those presented in this work and would not give origin to decays following a power law. For this reason the incontestable proof for the mechanism suggested in the **Figure 5** is yet to be found. However, we experimental evidence is clearly gathering that support this to be a viable mechanism to explain the power-law region appearing in the delayed fluorescence decay of exciplexes.

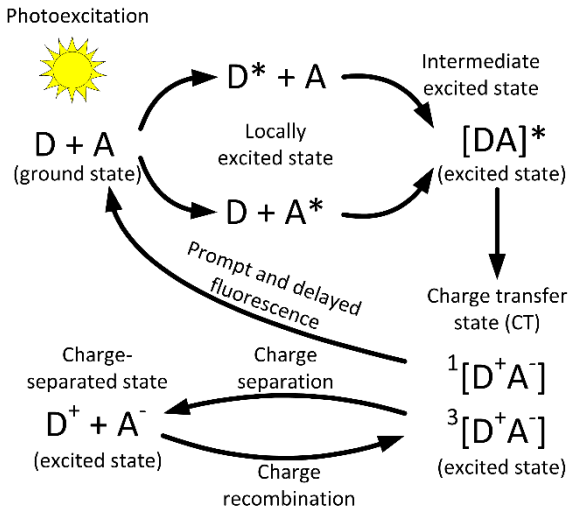

Figure 5. Model of photoexcited exciplex blend. Upon absorption of light, the donor (D) or/and acceptor (A) species form an excited state. The excited state molecule interacts with the ground state counterpart to form an excited state complex. A further step is electron transfer that results in the formation of CT states. The CT state can then undergo radiative or non-radiative decay. Another evolution pathway of the CT state is dissociation into free charge carriers. Holes and electrons migrate all over the D-A blend and eventually recombine giving again CT exciplex states.

Addressing the exciplex TADF behaviour. As the different exciplex decay regions have now been clarified on the basis of the available results, the differences observed in the exciplexes studied here can be more easily explained: (1) The blue-emitting exciplexes mCP:PO-T2T; CzSi:PO-T2T; and mCPPO1:PO-T2T are type (II) TADF character. All show visible and strong TADF contribution and a power law decay component is only observed at later times. This is in full agreement with the mechanism explained above, as the ^{1}CT/^{3}CT states are in near resonance with the ^{3}LE state and, therefore, the RISC rate is sufficiently fast to rapidly promote long-lived triplet states into emissive singlets. (2) The green emitting exciplexes, TSBPA:PO-T2T and TCBPA:PO-T2T show even higher TADF contribution than the blue emitting exciplexes, and

both show power law decays at later times. (3) The orange-yellow exciplexes, TPD:PO-T2T and NPB:PO-T2T, show a decreased amount of TADF contribution in relation to the prompt emission, and the power law decay becomes more pronounced. Finally, (4) the least energetic orange-red exciplex, DNTPD:PO-T2T, shows no visible contribution of TADF emission and the prompt fluorescence is directly followed by the power law decay. This clearly shows that the DNTPD:PO-T2T blend does not show any classical delayed fluorescence phenomena, but only a delayed fluorescence originated from non-geminate charge-recombination.

The luminescence that is generated from bimolecular charge-recombination is in principle identical with electroluminescence and as such also does not contribute to the triplet harvesting in the OLED device (assuming triplet harvesting is not effective). In this way, the exciplexes showing only prompt fluorescence and power-law decay will behave like any pure fluorescent emitter in OLEDs, showing very limited triplet harvesting. The observation of power law and exponential delayed fluorescence decays, therefore, must be distinguished from each other and special care must be taken not to assign the observation of a power law decay to the presence of "multiexponential decaying delayed fluorescence" as this is misleading and may hide a more general phenomenon that contributes to decreasing device efficiency (**Figure 6**, **S3-S18, S22-S29**).

Our results are remarkably in the way that some of the exciplexes studied here show very short delayed fluorescence lifetimes. For example, the TADF lifetimes of mCP:PO-T2T, TSBPA:PO-T2T and TCBPA:PO-T2T exciplexes are roughly 2 µs, and are among the shortest values reported for TADF emitters.[44–46] A short TADF lifetime is important to facilitate obtaining high EQE in OLEDs with decreasing efficiency roll-off, as it decreases the probability of triplet-triplet

annihilation and triplet-polaron quenching, which are causes of device efficiency roll-off often observed at high brightness.

It is also worth to note that the longest delayed fluorescence lifetime of 6.3 ± 0.3 μ and the smallest k_{RISC} constant of $1.1 \cdot 10^6$ s^{-1} are observed in CzSi:PO-T2T which is the consequence of the largest singlet-triplet gap in this blend. The S-T gap of CzSi:PO-T2T is calculated as the difference between the relaxed CT energy and the ^3LE_A energy, and equals 0.10 eV in this blend. For mCP:PO-T2T and mCPPO1:PO-T2T S-T singlet-triplet energy gaps below 0.01-0.02 eV are observed, which is within the margin of error in our determination. These exciplexes show much shorter lifetimes of *ca*. 2-3 μs and moderate k_{RISC} values of $2.7\text{-}3.2 \cdot 10^6$ s^{-1}. Consequently, the TCBPA:PO-T2T and TSBPA:PO-T2T exciplexes are expected to have virtually zero S-T gap due to the nearly zero ^{1}CT-^{3}CT energy barrier[17,21,23,47] (see text below for more details). These exciplexes show also very short TADF lifetime, ca. 2 μs, and have the highest TADF contribution, and faster k_{RISC} constants of $7.2\text{-}7.3 \cdot 10^6$ s^{-1} (also see **Table S5**). TPD:PO-T2T and NPB:PO-T2T show the shortest TADF lifetime among all the exciplexes studied here, with TADF decaying with a time constant of just 600 ns. Unfortunately, this is mainly due to increased non-radiative decay affecting the triplet state, as also the DF/PF ratio dramatically decreases[48,18] (**Table 1**, **Table S5, Figures S3-S18**).

It is notable that no evidence exists to support the observation of phosphorescence at 80K in any of the exciplex blends (except CzSi:PO-T2T, see text below). This is an indication that the singlet-triplet energy gap in these exciplexes is in general very narrow and therefore RISC dominates, even at low temperature. However, an additional weak emission is observed at long delay times, in the CzSi:PO-T2T blend at 80K, which is probably due to the phosphorescence of

PO-T2T. This is most likely the consequence of the largest singlet-triplet gap, 0.1 eV, in this blend which slows the RISC rate.

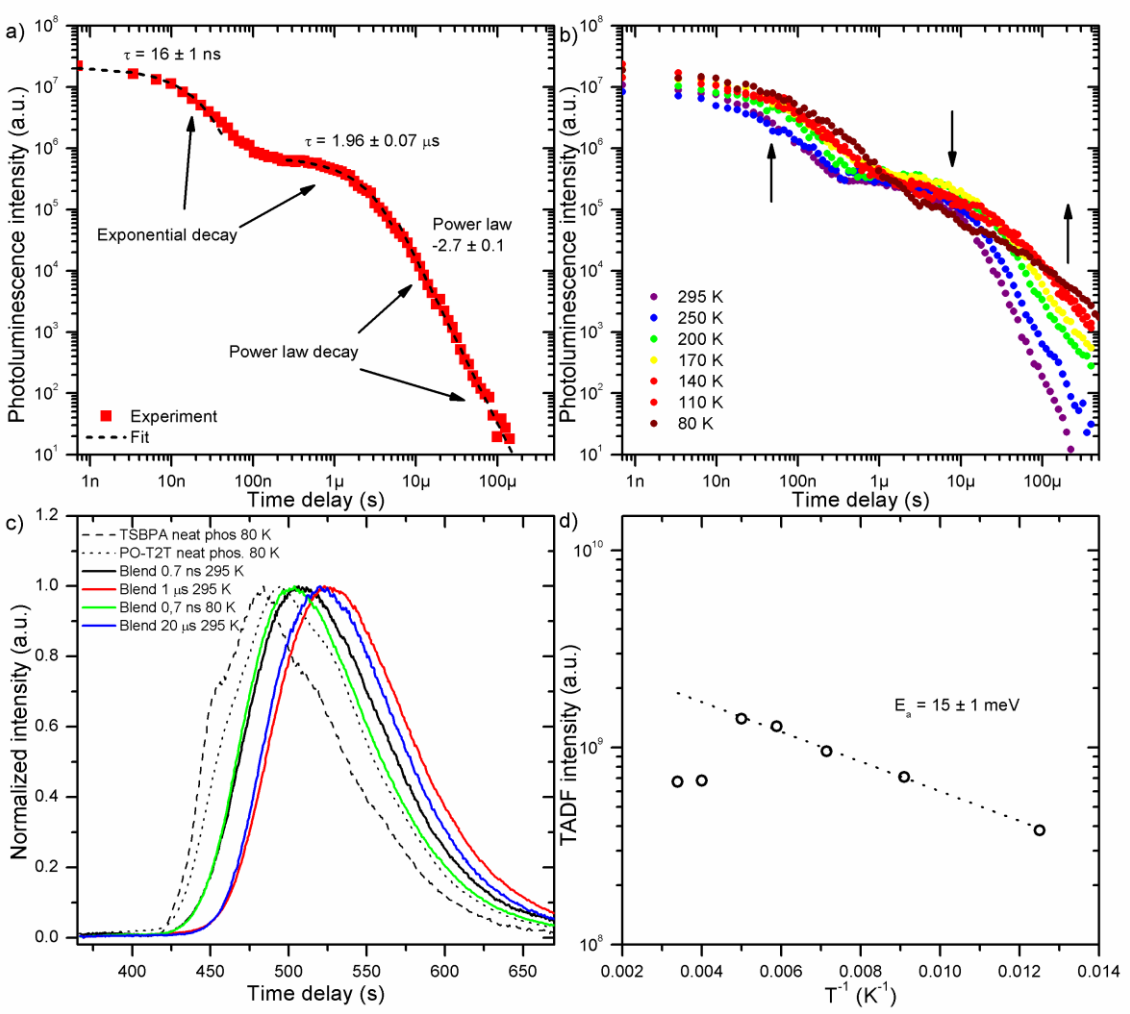

Figure 6. a) Photoluminescence decay of mCP:PO-T2T exciplex with fitted decay components. Note the decay components: exponential prompt and delayed fluorescence decay and power-law decay are indicated with arrows; b) photoluminescence decays of CzSi:PO-T2T exciplex at various temperatures. Notable changes to the decay upon temperature decrease are highlighted with arrows; c) prompt and delayed fluorescence spectra of TSBPA:PO-T2T exciplex with phosphorescence spectra of donor and acceptor species for comparison; d) temperature

dependence of TADF intensity for mCP:PO-T2T exciplex. Recorded in a vacuum (at 295 K) or in nitrogen at any other temperature.

In all the exciplexes herein (except for the obvious case of DNTPD:PO-T2T) the prompt emission is significantly blue shifted in relation to the delayed fluorescence. Interestingly, while the shape of the spectrum is preserved, the position of the emission intensity peak shows a gradual red-shift over time (see **Figures S3-S18** in SI).The time-dependence of this red-shift in the prompt-fluorescence region resembles an exponential decay, (see **Figures S3-S18**). This is clear evidence of the CT state relaxation. However, such relaxation may be related to changes in the D-A distance or in their relative orientation, occurring within the first 100 ns. It is, therefore, concluded that the prompt fluorescence mostly occurs from a non-relaxed CT state, whereas the TADF component is mainly produced from nearly relaxed exciplex states. For this reason, the CT emission that is observed around 1-10μs is the one used for the purpose of explaining the TADF phenomena in the exciplexes studied here, instead of the prompt or steady-state emissions. It is worth to note that the spectrum continuously but slowly red-shifts along the TADF and power law regions.

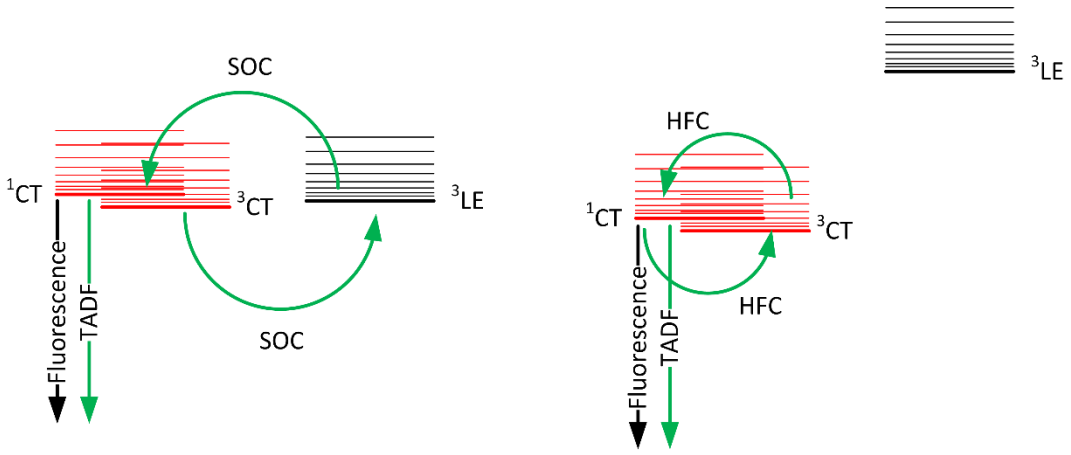

TADF in exciplex with CT being in resonance with ^{3}LE

TADF in exciplex with ^{3}LE out of resonance

Figure 7. Schematic diagram showing how TADF emission is generated in exciplexes with CT – ^{3}LE exchange (left) and without this exchange (right). SOC (spin-orbit coupling) and HFC (hyperfine coupling) indicate the major interactions in each case.

Explaining strong TADF in exciplexes without the involvement of ^{3}LE states. At this point, it is important to explain how the ^{1}CT - ^{3}CT exchange can be efficient without the involvement of a local ^{3}LE state acting as an intermediate. This is highly relevant for the understanding of the TADF mechanism, since the ^{1}CT - ^{3}CT transition is in general forbidden by symmetry and no TADF should be observed without involvement of local triplet states. However in systems where the 1CT and 3CT states are almost degenerate, hyperfine coupling interaction (HFC) may provide fast enough spin exchange to promote ISC and RISC (**Figure 7**).[49,50] In fact, HFC does not require any activation energy as ^{1}CT and ^{3}CT are nearly isoenergetic, but is only effective for very small S-T energy splitting. In our exciplex systems, the TADF emission shows a temperature-activated regime with an energy barrier of 11-35 meV. This is clearly too large for the ^{1}CT - ^{3}CT energy difference, but it is within the range of energy associated with molecular rotational and vibrational transitions. Therefore, we speculate that the ^{1}CT - ^{3}CT transition associated with HFC may involve crossing from upper vibrational levels of the ^{3}CT state. More importantly, and to conclude this section, our results indicate that regardless of the location of the ^{3}LE state, above or in line with the CT state, the conditions are favourable for TADF because the ^{3}CT state lives long enough in order for efficient RISC to occur. This is the case in TSBPA:PO-T2T and TCBPA:PO-T2T exciplexes. On the other hand, having the ^{3}LE state below the CT state may be not beneficial for TADF. In fact, the ^{3}LE state may even act as a trap and favoring TADF quenching when is too far below the CT state. Note that the activation energy of TADF in TCBPA:PO-T2T and TSBPA:PO-T2T exciplexes is in the range of 10-20 meV, which

is significantly lower than the energy difference between the relaxed CT and the lowest local triplet that is 200-300 meV. This undoubtedly demonstrates that the role of the local triplet state is not as crucial in these exciplexes as it has been reported previously in intramolecular systems.[33]

Devices (OLED Characterization). To investigate the charge transfer complexes under electrical excitation, all studied exciplexes have been implemented in OLED structures. The structures of the fabricated devices were as follows: ITO/ NPB (10nm)/ TCTA(10nm)/ CzSi(5nm)/ **CzSi:PO-T2T**(20nm)/ PO-T2T(50nm)/ LiF (1nm)/Al (100nm) (**B1**); ITO/ NPB (10nm)/ TCTA(10nm)/ mCP(5nm)/ **mCP:PO-T2T**(20nm)/ PO-T2T(50nm)/ LiF (1nm)/Al (100nm) (**B2**); ITO/ NPB (30nm)/ TCTA(10nm)/ mCPPO1(5nm)/ **mCPPO1:PO-T2T**(20nm)/ PO-T2T(50nm)/ LiF (1nm)/Al (100nm) (**B3**); ITO/ NPB(30nm)/ TSBPA(10nm)/ **TSBPA:PO-T2T** (20nm)/ PO-T2T(50nm)/ LiF(1nm)/ Al (100nm) (**G1**); ITO/ NPB(40nm)/ TCBPA(10nm)/ **TCBPA:PO-T2T** (20nm)/ PO-T2T(60nm)/ LiF(1nm)/ Al (100nm) (**G2**); ITO/ TAPC (20nm)/NPB (10nm)/ **NPB:PO-T2T** (20nm)/ PO-T2T(50nm)/ LiF (1nm)/ Al (100nm) (**O1**); ITO/ TAPC (40nm)/TPD (10nm)/ **TPD:PO-T2T** (20nm)/ PO-T2T(50nm)/ LiF (1nm)/ Al (100nm) (**O2**); ITO/ NPB (30nm)/ DNTPD (10nm)/ **DNTPD:PO-T2T** (20nm)/ PO-T2T (50nm)/ LiF (1nm)/ Al (100nm) (**R1**). The chemical structures of exciplex forming materials used in devices are shown in **Figure 1** and the schematic representation of the structure of the devices is shown in **Figure S20**. **Figure 8** shows the normalized EL spectra of fabricated devices using the different exciplexes as the emitting layer. In all cases, the EL spectra are similar to the PL spectra obtained in the blends of the donor and acceptor molecules. It should be noted that the emission of OLEDs does not contain emission from ETL or HTL layers, which indicates that the excitons are confined in the emission layer without leakage to the adjacent layers. The peak

intensities of the EL spectra with the full characteristics of the exciplex based devices (**Figure 8b, Figure S21**) are summarized in **Table 2** (**Tables S2-S4**). The turn-on voltage is very low in all of the devices studied (2.5-4V), which suggests that the charge carriers are injected from the electrodes and transported to the emitting exciplex states without significant energy barriers. Furthermore, the EL spectra remain stable with increasing driving voltage.

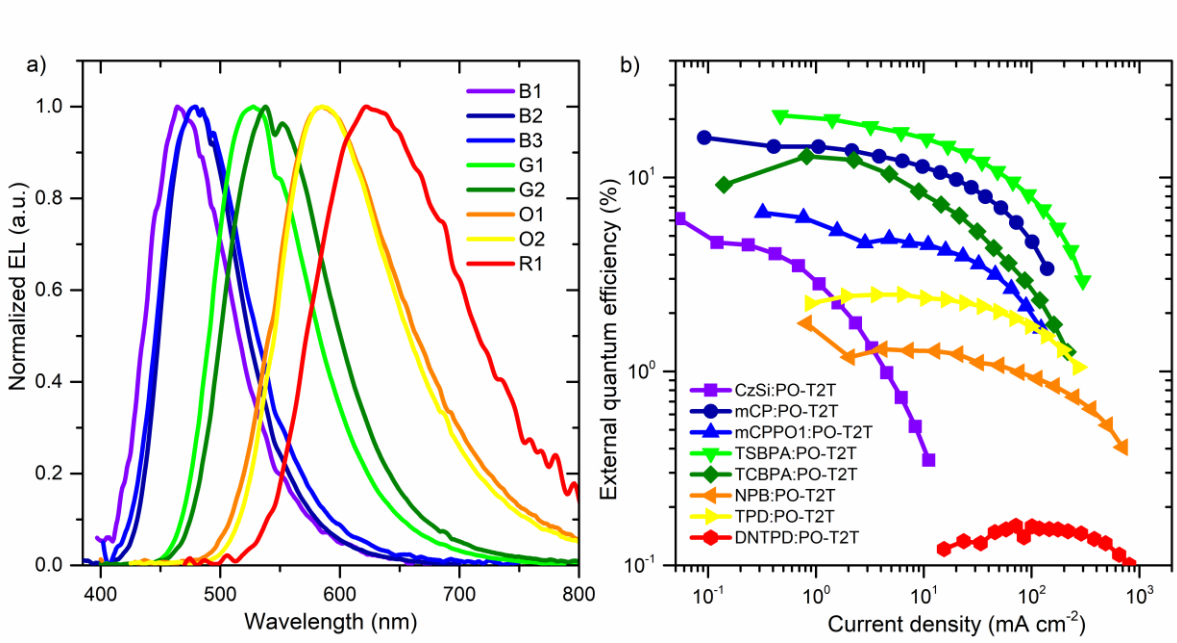

Figure 8. a) Electroluminescence spectra of fabricated devices; b) external quantum efficiency of fabricated devices. Note: donor-acceptor ratio is 1:1 in all emissive layers.

In the group of the blue OLEDs (B1-B3) the deepest blue emission is obtained from an OLED made with CzSi:PO-T2T exciplex (device B1), with the EL spectra peaking at 465 nm and with CIE colour coordinates (0.16; 0.21). The current efficiency (η_L), power efficiency (η_P), and external quantum efficiency (η_{ext}) of CzSi:PO-T2T OLEDs are 8 cd A^{-1}, 5.8 lm $W^{-1,}$ and 4.7%, respectively. All these parameters were determined at a brightness level of 100 cd m^{-2}. The blue exciplex OLED realizes a maximum EQE of 6.1%, which is one of the best values for deep blue

exciplex OLEDs.[51,15] However, the device B1 with the deepest blue colour in this work showed high-efficiency roll-off at high current density. This observation is explained by the longest delayed fluorescence lifetime of this exciplex consistent with the largest singlet-triplet splitting in this system (**Table 1**). Such emitting system can be used in SSL technology for improved colour rendering index (CRI) and co-host for TADF or phosphorescence OLEDs due to high triplet levels of these materials. The two other blue devices (B2 and B3) were fabricated with mCP:PO-T2T and mCPPO1:PO-T2T exciplexes. These devices show similar EL spectra peaking at 480 nm, and chromaticity coordinates of (0.16; 0.28) and (0.18; 0.29), respectively, corresponding to sky-blue colour. As shown in **Table 2**, the mCP:PO-T2T OLED shows one of the best performances, with a η_{ext} of 14.5 % and η_L=26.7 cd A^{-1}, and η_p=24 lm W^{-1}, at 100 cd m^{-2}, and η_{ext} of 12.9 % with η_L= 24.6 cd A^{-1}, η_p=15 lm W^{-1} at 1000 cd m^{-2} brightness. It is already known from previous studies that mCP:PO-T2T is an efficient emitting system, which has been used as a host for phosphorescent dopants.[15,16] Remarkably, the performances presented in this work are among the best parameters for optimized sky-blue exciplex OLEDs that have been reported so far. The device B3, fabricated with the mCPPO1:PO-T2T blend, shows also a good performance with η_L of 9.5 cd A^{-1}, η_P of 7.5 lm W^{-1} and η_{ext} of 6.3% at 100 cd m^{-2}, and η_{ext}= 4.5 %, η_L=8.8 cd A^{-1}, and η_p=4.3 lm W^{-1} at 1000 cd m^{-2}. At first glance, device B3 exhibits maximum η_{ext} =6.5% in comparison with device B2, where $\eta_{ext\ max}$=16%. The maximum brightness of device B3 reached 3920 cd m^{-2} at 10V while that of the device B2 was 8960 cd m^{-2}. Although mCPPO1 shows lower hole mobility[52] than mCP, it is evident that the lower Φ_{PL} of the mCPPO1:PO-T2T exciplex blend explains the difference in efficiency between devices B2 and B3 (**Table S5**). Additionally, the unbalanced hole and electron concentration in the emitting layer due to the bipolar nature of mCPPO1 may adversely affect the efficiency of the exciton

formation. In fact, in device B3 the application of thicker HIL, to enhance hole transport, was necessary. At the same time, OLEDs showed a low driving voltage (3V) in consequence of the exciton confinement geometry in these devices where the charge carrier recombination process occurs in the exciplex forming region.

Table 2. Summary of OLEDs performance: turn-on voltage (V_{on}), maximum brightness (L_{max}) and current efficiency ($\eta_{L,max}$), maximum power efficiency ($\eta_{P,max}$) and external quantum efficiency ($\eta_{ext,\,max}$), maxima of EL (λ_{max}) spectra and CIE 1931 color coordinate and current efficiency (η_L), power efficiency (η_P), external quantum efficiency (η_{ext}) at 100 cd m^{-2} and 1000 cd m^{-2} brightness.

		V_{on}	L_{max} (cd m^{-2})	$\eta_{L,max}$ (cd A^{-1})	$\eta_{P,max}$ (lm W^{-1})	$\eta_{ext,\,max}$ (%)	λ_{max} EL (nm)	CIE 1931 (x; y)	100 cd m^{-2}		1 000 cd m^{-2}	
									η_L, (cd A^{-1})	η_{ext} (%)	η_L, (cd A^{-1})	η_{ext} (%)
CzSi:PO-T2T	**B1**	3	900	8.9	7	6.1	465	(0.16;0.21)	8	4.7	-	-
mCP: PO-T2T	**B2**	3	8960	27	26.4	16	480	(0.16;0.28)	26.7	14.5	24.6	12.9
mCPPO1: PO-T2T	**B3**	3	3920	9.4	8	6.5	480	(0.18;0.29)	9.5	6.3	8.8	4.5
TSBPA:PO-T2T	**G1**	2.5	31000	60.9	71	20	528	(0.33;0.57)	57	19	60	18
TCBPA: PO-T2T	**G2**	2.5	9070	43.7	45.8	12.8	542	(0.38;0.56)	38	10	40	12
TPD: PO-T2T	**O1**	3.5	6165	5	4.8	2.4	585	(0.53;0.47)	5.3	2.4	4.7	2.1
NPB: PO-T2T	**O2**	3	6080	2.4	2.1	1.7	585	(0.52;0.46)	2.2	1.3	2	1

DNTPD: PO-T2T	**R1**	4	925	0.1	0.05	0.15	628	(0.60;0.39)	0.14	0.14	-	-

The group of green emitting OLEDs, TSBPA:PO-T2T (G1) and TCBPA:PO-T2T (G2) have shown perfect triplet harvesting. Notably, device G1 showed an extremely high η_L of 57 cd A^{-1}, η_P of 67 lm W^{-1} and η_{ext} of 19% at 100 cd m^{-2}, (60 cd A^{-1}, 54 lm W^{-1}, η_{ext} 18% at 1000 cd m^{-2}), with extremely low driving voltage. To our knowledge, these values represent the best performance in exciplex based OLEDs without using any outcoupling enhancement, which is very close to the state-of-the-art conventional (any other not using exciplex as an emitter) TADF OLEDs.[19] The excellent performance of TSBPA:PO-T2T devices is due to the high hole mobility of TSBPA[53], its high triplet level (2.9 eV) and singlet-triplet energy gap close to zero, as confirmed by the photophysical time-resolved measurements. The maximum intensity of the EL spectrum observed for device G1, 528 nm, appears shifted by 15 nm to the blue when compared with the PL spectrum of TSBPA:PO-T2T, however, the emission *onset* remains the same. Such shift is attributed to the effect of the electric field in the exciplex or because of a larger contribution of the shorter-lived components of the TADF electroluminescence in relation to photoluminescence, due to the initial populations of singlet and triplet states under electrical excitation.[4,54] Although both green exciplexes were very similar from the photophysical point of view, the performance of the device (G2) was slightly worse than the device G1. At 100 cd m^{-2} device G2 shows η_L of 38 cd A^{-1}, η_P of 44 lm W^{-1} and η_{ext} = 10%, (40 cd A^{-1}, 36 lm W^{-1}, η_{ext} 12% at 1000 cd m^{-2}). The reason for the relatively lower efficiency of device G2, when compared with device G1 could be due to the formation of an electromer, due to the presence of defect sites in TCBPA that may act as deep electron traps.[55,56] Therefore, when using TCBPA as HTL, OLEDs should be carefully designed to avoid emission from electromers, by shifting the

emission region far enough from TCBPA. However, both G1 and G2 OLEDs exhibit low turn-on voltage (2.5V) and high performance which indicate effective triplet harvesting due to TADF with nearly 100% efficiency. The chromaticity coordinates (x, y) of devices G1 and G2 were found to be (0.33 ;0.57) and (0.38; 0.56), respectively.

Finally, the third group of devices exhibited emission in the orange-red region of the visible spectrum. Employing efficient orange-red exciplexes in OLEDs is an urgent task for developing organic solid-state lighting (SSL).[2] The devices O1 and O2 show identical electroluminescence spectra with emission at 585 nm and similar CIE colour coordinates, (0.52;0.46) for NPB:PO-T2T and (0.53;0.47) for TPD:PO-T2T. At a brightness level of 100 cd m^{-2}, the O1 and O2 devices show η_L of 2.2 cd A^{-1}, η_P of 1.9 lm W^{-1}, η_{ext} of 1.3% for NPB:PO-T2T, and η_L of 5.3 cd A^{-1}, η_P of 3.9 lm W^{-1}, η_{ext} of 2.4% for TPD:PO-T2T. Maximum external quantum efficiencies of 1.7% and 2.4% were obtained for NPB:PO-T2T and TPD:PO-T2T OLEDs, respectively. These values are due to the low contribution of TADF caused by the significant internal conversion that affects the triplet population in both exciplexes. Nevertheless, the maximum brightness of both devices reached 6 000 cd m^{-2} at 10V. In our study, using DNTPD:PO-T2T (R1) as the emitter we observed the orange-red exciplex emission with the EL maximum at 628 nm and CIE 1931 chromaticity coordinates of (0.60; 0.39). Maximum values of η_L, η_P, and η_{ext} equal to 0.14 cd A^{-1}, 0.07 lm W^{-1}, and 0.14%, respectively, were obtained. As expected, the DNTPD:PO-T2T exciplex did not exhibit any TADF phenomena and behaved like a typical fluorescence emitter.

In summary, the OLEDs demonstrate extremely low turn-on voltage (2.5-3.5V) and achieve high brightness (~5000 cd m^{-2}) at low current density. Both these are crucial parameters in display and lighting applications. Indeed in display (or SSL) technology or in a tandem device, single pixels need to be operated at a low current density.

CONCLUSIONS

The photophysics of eight different non-doped exciplex blends were investigated and OLEDs fabricated that show remarkably device performances. A clear correlation is obtained between the photophysical parameters of the exciplexes and their device efficiency in terms of the TADF emission. OLEDs based on TSBPA:PO-T2T exciplex showed a green TADF emission with record high $\eta_{L,\ max}$ of 60.9 (cd A^{-1}), $\eta_{P,\ max}$ of 71 (lm W^{-1}) and $\eta_{ext,\ max}$ of 20%, which is close to the maximum theoretical values. Efficient multi-colour exciplexes, as the ones shown in this work represent a clear move towards the fabrication of exciplex-based efficient lighting at lower cost, as joining chosen multi-colour exciplexes in one device may give different shades of white. We believe this work gives further evidence to explain the photophysical behavior of uni- and bimolecular TADF emitters, and opens a pathway for relatively not well established TADF emitters to be explored in OLEDs, where multi-colour non-doped TADF exciplexes can be used to fabricate OLEDs covering the entire visible emission range, from blue to red, without using host materials, and thus saving on fabrication costs.. We believe our work will give a novel insight for the future development of OLED technology based on exciplexes with high efficiency and simplified structure of devices.

EXPERIMENTAL SECTION

Photophysics. Photoluminescence spectra of thin films were recorded at room temperature with Edinburgh Instruments FLS980 fluorescence spectrometer with Xe-lamp as an excitation source and R-928 photomultiplier detector. Phosphorescence, prompt fluorescence (PF), and delayed fluorescence (DF) spectra and decays were recorded using nanosecond gated luminescence and lifetime measurements (from 400 ps to 1 s) using either third harmonics of a high energy pulsed Nd:YAG laser emitting at 355 nm (EKSPLA) or a N_2 laser emitting at 337

nm. Emission was focused onto a spectrograph and detected on a sensitive gated iCCD camera (Stanford Computer Optics) having a sub-nanosecond resolution. PF/DF time-resolved measurements were performed by exponentially increasing gate and integration times. Temperature-dependent experiments were conducted using a continuous flow liquid nitrogen cryostat (Janis Research) under a nitrogen atmosphere. Photoluminescence quantum yield of thin films was recorded using a QePro spectrometer (Ocean Optics) coupled with an integrating sphere (Labsphere) and LED light source (Ocean Optics) using a method described elsewhere[57].

Devices. OLEDs have been fabricated on pre-cleaned, patterned indium-tin-oxide (ITO) coated glass substrates with a sheet resistance of 20 Ω/sq and ITO thickness of 100 nm. All small molecules and cathode layers were thermally evaporated in Kurt J. Lesker Spectros II evaporation system under pressure of 10^{-6} mbar without breaking the vacuum. The sizes of pixels were 8 mm^2 and 16 mm^2. NPB (*N*,*N*′-di(1-naphthyl)-*N*,*N*′-diphenyl-(1,1′-biphenyl)-4,4′-diamine), TCTA (Tris(4-carbazoyl-9-ylphenyl)amine) or TAPC (4,4′-Cyclohexylidenebis[*N*,*N*-bis(4-methylphenyl)benzenamine]) were used as a Hole Injection Layer (HIL) and Hole Transport Layer (HTL). PO-T2T (2,4,6-Tris[3-(diphenylphosphinyl)phenyl]-1,3,5-triazine) was introduced as a Hole Blocking Layer (HBL) and Electron Transport Layer (ETL). Lithium fluoride (LiF) and aluminium were used as the cathode. Organic semiconductors and aluminium were deposited at a rate of 1 $Å s^{-1}$, and the LiF layer was deposited at 0.1 $Å s^{-1}$. In case of electron donating (D) materials for exciplex have been used: CzSi (9-(4-tert -butylphenyl)-3,6-bis(triphenylsilyl)-9*H*-carbazole), mCP (1,3-Bis(carbazol-9-yl)benzene), mCPPO1 (9-(3-(9*H*-Carbazol-9-yl)phenyl)-3-(diphenylphosphoryl)-9*H*-carbazole), TSBPA (4,4'-(Diphenylsilanediyl)bis(*N*,*N*-diphenylaniline)), TCBPA (4,4'-(Diphenylmethylene)bis(*N*,*N*-diphenylaniline)), NPB, TPD (*N*,*N*′-Bis(3-methylphenyl)-*N*,*N*′-diphenylbenzidine), DNTPD

(*N*1,*N*1'-(Biphenyl-4,4'-diyl)bis(*N*1-phenyl-*N*4,*N*4-di-m-tolylbenzene-1,4-diamine)) and electron-accepting PO-T2T. Each emitting layer has been formed by co-deposition of donor and acceptor at the identical rate (1:1 ratio)[20]. The characteristics of the devices were recorded using 10-inch integrating sphere (Labsphere) connected to a Source Meter Unit and Ocean Optics USB4000 spectrometer[58]. All materials were purchased from Sigma Aldrich or Lumtec and were purified by temperature-gradient sublimation in a vacuum.

Electrochemistry. Electrochemical measurements were performed in 0.1 M Bu_4NPF_6 (99%, Sigma Aldrich, dried) in dichloromethane (CHROMASOLV®, 99.9% Sigma Aldrich). Solutions were purged with argon prior to measurement. Electrodes: working (Pt disc 1 mm of diameter), counter (Pt wire), reference (Ag/Ag^+ in dichloromethane/0.1 M Bu_4NPF_6 solution, calibrated against ferrocene). All cyclic voltammetry measurements performed at room temperature with a scan rate of 50 mV s^{-1}. Ionization potential (IP) and electron affinity (EA) were calculated from *onset* oxidation (E_{ox}) and reduction (E_{red}) potentials, respectively, using following equations: IP = E_{ox} + 5.1, EA = E_{red} + 5.1[59,60]. Detailed description of the experimental technique can be found elsewhere.[61]

ASSOCIATED CONTENT

Supporting Information. The Supporting Information is available free of charge on the ACS Publications website at DOI: 10.xxxx/acsami.xxxxx.

Absorption and PL spectra of the donors (D) and acceptor (A) and of their blends, time-resolved measurements of exciplex blends, phosphorescence spectra of D and A molecules, electrochemistry data, energy band diagrams of OLEDs and devices performance and discussions (PDF)

AUTHOR INFORMATION

Corresponding Author

* Dr. Przemyslaw Data. E-mail: przemyslaw.data@durham.ac.uk.

* Dr. Fernando B. Dias. E-mail: f.m.b.dias@durham.ac.uk.

* Dr. Gabriela Wiosna-Salyga. E-mail: gabriela.wiosna-salyga@p.lodz.pl.

ORCID

Piotr Pander: 0000-0003-4103-4154

Fernando B. Dias: 0000-0001-9841-863X

Przemyslaw Data: 0000-0002-1831-971X

Author Contributions

The manuscript was written through contributions of all authors. All authors have given approval to the final version of the manuscript. [§]These authors contributed equally to the experimental work.

Notes

The authors declare no competing financial interest.

ACKNOWLEDGMENT

This work was supported by the EXCILIGHT project funded by the European Union's Horizon 2020 Research and Innovation Programme under grant agreement No. 674990. P.D. acknowledges the Polish National Science Centre funding, grant no. 2017/25/B/ST5/02488.

REFERENCES

1 M. Y. Wong and E. Zysman-Colman, *Adv. Mater.*, 2017, **29**, 1605444.

2 D. D. S. Pereira, P. L. dos Santos, J. S. Ward, P. Data, M. Okazaki, Y. Takeda, S. Minakata, M. R. Bryce and A. P. Monkman, *Sci. Rep.*, 2017, **7**, 6234.

3 P. L. dos Santos, J. S. Ward, M. R. Bryce and A. P. Monkman, *J. Phys. Chem. Lett.*, 2016, **7**, 3341–3346.

4 K. Goushi, K. Yoshida, K. Sato and C. Adachi, *Nat. Photonics*, 2012, **6**, 253–258.

5 J. Kalinowski, M. Cocchi, D. Virgili, V. Fattori and J. A. G. Williams, *Adv. Mater.*, 2007, **19**, 4000–4005.

6 M. Cocchi, D. Virgili, C. Sabatini and J. Kalinowski, *Chem. Phys. Lett.*, 2006, **421**, 351–355.

7 M. Sarma and K.-T. Wong, *ACS Appl. Mater. Interfaces*, 2018, acsami.7b18318.

8 T.-L. Wu, M.-J. Huang, C.-C. Lin, P.-Y. Huang, T.-Y. Chou, R.-W. Chen-Cheng, H.-W. Lin, R.-S. Liu and C.-H. Cheng, *Nat. Photonics*, 2018, **12**, 235–240.

9 H. Kaji, H. Suzuki, T. Fukushima, K. Shizu, K. Suzuki, S. Kubo, T. Komino, H. Oiwa, F. Suzuki, A. Wakamiya, Y. Murata and C. Adachi, *Nat. Commun.*, 2015, **6**, 8476.

10 H. Uoyama, K. Goushi, K. Shizu, H. Nomura and C. Adachi, *Nature*, 2012, **492**, 234–238.

11 W. Zeng, H.-Y. Lai, W.-K. Lee, M. Jiao, Y.-J. Shiu, C. Zhong, S. Gong, T. Zhou, G. Xie, M. Sarma, K.-T. Wong, C.-C. Wu and C. Yang, *Adv. Mater.*, 2018, **30**, 1704961.

12 S. Wang, X. Yan, Z. Cheng, H. Zhang, Y. Liu and Y. Wang, *Angew. Chemie Int. Ed.*, 2015, **54**, 13068–13072.

13 Y. Wada, S. Kubo and H. Kaji, *Adv. Mater.*, 2018, **30**, 1705641.

14 D.-H. Kim, A. D'Aléo, X.-K. Chen, A. D. S. Sandanayaka, D. Yao, L. Zhao, T. Komino, E. Zaborova, G. Canard, Y. Tsuchiya, E. Choi, J. W. Wu, F. Fages, J.-L. Brédas, J.-C. Ribierre and C. Adachi, *Nat. Photonics*, 2018, **12**, 98–104.

15 X.-K. Liu, Z. Chen, J. Qing, W.-J. Zhang, B. Wu, H. L. Tam, F. Zhu, X.-H. Zhang and C.-S. Lee, *Adv. Mater.*, 2015, **27**, 7079–7085.

16 J.-H. Lee, S.-H. Cheng, S.-J. Yoo, H. Shin, J.-H. Chang, C.-I. Wu, K.-T. Wong and J.-J. Kim, *Adv. Funct. Mater.*, 2015, **25**, 361–366.

17 W. Hung, G. Fang, Y. Chang, T. Kuo, P. Chou, S. Lin and K. Wong, *ACS Appl. Mater. Interfaces*, 2013, **5**, 6826–6831.

18 K.-H. Kim, S.-J. Yoo and J.-J. Kim, *Chem. Mater.*, 2016, **28**, 1936–1941.

19 W. Liu, J.-X. Chen, C. Zheng, K. Wang, D. Chen, F. Li, Y.-P. Dong, C.-S. Lee, X.-M. Ou and X.-H. Zhang, *Adv. Funct. Mater.*, 2016, **26**, 2002–2008.

20 W. Hung, T. Wang, P. Chiang, B. Peng and K. Wong, *ACS Appl. Mater. Interfaces*, 2017, **9**, 7355–7361.

21 T. Zhang, B. Chu, W. Li, Z. Su, Q. M. Peng, B. Zhao, Y. Luo, F. Jin, X. Yan, Y. Gao, H.

Wu, F. Zhang, D. Fan and J. Wang, *ACS Appl. Mater. Interfaces*, 2014, **6**, 11907–11914.

22 V. Jankus, P. Data, D. Graves, C. McGuinness, J. Santos, M. R. Bryce, F. B. Dias and A. P. Monkman, *Adv. Funct. Mater.*, 2014, **24**, 6178–6186.

23 D. Graves, V. Jankus, F. B. Dias and A. Monkman, *Adv. Funct. Mater.*, 2014, **24**, 2343–2351.

24 P. L. Dos Santos, F. B. Dias and A. P. Monkman, *J. Phys. Chem. C*, 2016, **120**, 18259–18267.

25 P. Pander, A. Kudelko, A. Brzeczek, M. Wroblowska, K. Walczak and P. Data, *Disp. Imaging*, 2017, **2**, 265–277.

26 P. Data, R. Motyka, M. Lapkowski, J. Suwinski, S. Jursenas, G. Kreiza, A. Miasojedovas and A. P. Monkman, *Electrochim. Acta*, 2015, **182**, 524–528.

27 Z. Wu, L. Yu, F. Zhao, X. Qiao, J. Chen, F. Ni, C. Yang, T. Ahamad, S. M. Alshehri and D. Ma, *Adv. Opt. Mater.*, 2017, **5**, 1700415.

28 J.-H. Lee, H. Shin, J.-M. Kim, K.-H. Kim and J.-J. Kim, *ACS Appl. Mater. Interfaces*, 2017, **9**, 3277–3281.

29 W.-Y. Hung, G.-C. Fang, S.-W. Lin, S.-H. Cheng, K.-T. Wong, T.-Y. Kuo and P.-T. Chou, *Sci. Rep.*, 2015, **4**, 5161.

30 F. B. Dias, K. N. Bourdakos, V. Jankus, K. C. Moss, K. T. Kamtekar, V. Bhalla, J. Santos, M. R. Bryce and A. P. Monkman, *Adv. Mater.*, 2013, **25**, 3707–3714.

31 M. Gordon and W. R. Ware, Eds., *The Exciplex*, Academic Press, 1975.

32 P. Data, A. Kurowska, S. Pluczyk, P. Zassowski, P. Pander, R. Jedrysiak, M. Czwartosz, L. Otulakowski, J. Suwinski, M. Lapkowski and A. P. Monkman, *J. Phys. Chem. C*, 2016, **120**, 2070–2078.

33 F. B. Dias, J. Santos, D. R. Graves, P. Data, R. S. Nobuyasu, M. A. Fox, A. S. Batsanov, T. Palmeira, M. N. Berberan-Santos, M. R. Bryce and A. P. Monkman, *Adv. Sci.*, 2016, **3**, 1600080.

34 M. K. Etherington, J. Gibson, H. F. Higginbotham, T. J. Penfold and A. P. Monkman, *Nat. Commun.*, 2016, **7**, 13680.

35 M. K. Etherington, F. Franchello, J. Gibson, T. Northey, J. Santos, J. S. Ward, H. F. Higginbotham, P. Data, A. Kurowska, P. L. Dos Santos, D. R. Graves, A. S. Batsanov, F. B. Dias, M. R. Bryce, T. J. Penfold and A. P. Monkman, *Nat. Commun.*, 2017, **8**, 14987.

36 R. S. Nobuyasu, Z. Ren, G. C. Griffiths, A. S. Batsanov, P. Data, S. Yan, A. P. Monkman, M. R. Bryce and F. B. Dias, *Adv. Opt. Mater.*, 2016, **4**, 597–607.

37 C. M. Marian, *J. Phys. Chem. C*, 2016, **120**, 3715–3721.

38 B. T. Lim, S. Okajima, A. K. Chandra and E. C. Lim, *J. Chem. Phys.*, 1982, **77**, 3902–3909.

39 J. Gibson, A. P. Monkman and T. J. Penfold, *ChemPhysChem*, 2016, **17**, 2956–2961.

40 S. Hirata, Y. Sakai, K. Masui, H. Tanaka, S. Y. Lee, H. Nomura, N. Nakamura, M. Yasumatsu, H. Nakanotani, Q. Zhang, K. Shizu, H. Miyazaki and C. Adachi, *Nat. Mater.*, 2015, **14**, 330–336.

41 V. Cherpak, P. Stakhira, B. Minaev, G. Baryshnikov, E. Stromylo, I. Helzhynskyy, M. Chapran, D. Volyniuk, Z. Hotra, A. Dabuliene, A. Tomkeviciene, L. Voznyak and J. V. Grazulevicius, *ACS Appl. Mater. Interfaces*, 2015, **7**, 1219–1225.

42 R. Kabe and C. Adachi, *Nature*, 2017, **550**, 384–387.

43 T.-C. Lin, M. Sarma, Y.-T. Chen, S.-H. Liu, K.-T. Lin, P.-Y. Chiang, W.-T. Chuang, Y.-C. Liu, H.-F. Hsu, W.-Y. Hung, W.-C. Tang, K.-T. Wong and P.-T. Chou, *Nat. Commun.*, 2018, **9**, 3111.

44 F. B. Dias, T. J. Penfold and A. P. Monkman, *Methods Appl. Fluoresc.*, 2017, **5**, 12001.

45 Y. Tao, K. Yuan, T. Chen, P. Xu, H. Li, R. Chen, C. Zheng, L. Zhang and W. Huang, *Adv. Mater.*, 2014, **26**, 7931–7958.

46 W.-C. Chen, C.-S. Lee and Q.-X. Tong, *J. Mater. Chem. C*, 2015, **3**, 10957–10963.

47 B. Frederichs and H. Staerk, 2008, **460**, 116–118.

48 X. Wei, Y. Chen, R. Duan, J. Liu, R. Wang, Y. Liu, Z. Li, Y. Yi, Y. Yamada-Takamura, P. Wang and Y. Wang, *J. Mater. Chem. C*, 2017, **5**, 12077–12084.

49 A. M. Scott and M. R. Wasielewski, *J. Am. Chem. Soc.*, 2011, **133**, 3005–3013.

50 T. Ogiwara, Y. Wakikawa and T. Ikoma, *J. Phys. Chem. A*, 2015, **119**, 3415–3418.

51 M. Cekaviciute, J. Simokaitiene, D. Volyniuk, G. Sini and J. V. Grazulevicius, *Dye. Pigment.*, 2017, **140**, 187–202.

52 S. O. Jeon, S. E. Jang, H. S. Son and J. Y. Lee, *Adv. Mater.*, 2011, **23**, 1436–1441.

53 C. W. Lee and J. Y. Lee, *Synth. Met.*, 2013, **167**, 1–4.

54 H. A. Al Attar and A. P. Monkman, *Adv. Mater.*, 2016, **28**, 8014–8020.

55 J. Kalinowski, G. Giro, M. Cocchi, V. Fattori and P. Di Marco, *Appl. Phys. Lett.*, 2000, **76**, 2352–2354.

56 E. Angioni, M. Chapran, K. Ivaniuk, N. Kostiv, V. Cherpak, P. Stakhira, A. Lazauskas, S. Tamulevičius, D. Volyniuk, N. J. Findlay, T. Tuttle, J. V. Grazulevicius and P. J. Skabara, *J. Mater. Chem. C*, 2016, **4**, 3851–3856.

57 J. C. de Mello, H. F. Wittmann and R. H. Friend, *Adv. Mater.*, 1997, **9**, 230–232.

58 P. D. and A. P. M. Daniel de Sá Pereira, *Disp. Imaging*, 2017, **2**, 323–337.

59 C. M. Cardona, W. Li, A. E. Kaifer, D. Stockdale and G. C. Bazan, *Adv. Mater.*, 2011, **23**, 2367–2371.

60 P. Data, P. Pander, M. Lapkowski, A. Swist, J. Soloducho, R. R. Reghu and J. V. Grazulevicius, *Electrochim. Acta*, 2014, **128**, 430–438.

61 S. Pluczyk, M. Vasylieva and P. Data, *J. Vis. Exp.*, , DOI:10.3791/56656.

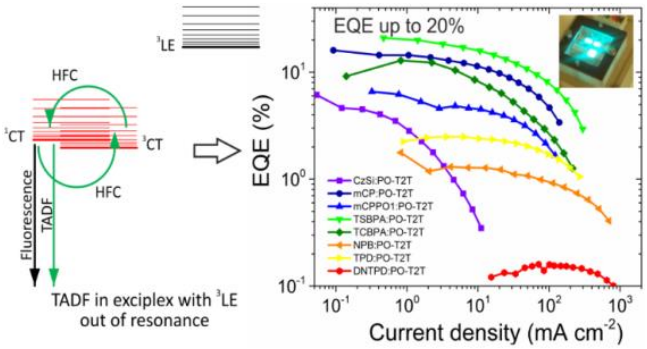
^{3}LE
HFC
^{1}CT
^{3}CT
HFC
Fluorescence
TADF
TADF in exciplex with ^{3}LE
out of resonance
EQE up to 20%
EQE (%)
10^1
10^0
10^{-1}
CzSi:PO-T2T
mCP:PO-T2T
mCPPO1:PO-T2T
TSBPA:PO-T2T
TCBPA:PO-T2T
NPB:PO-T2T
TPD:PO-T2T
DNTPD:PO-T2T
10^{-1}
10^0
10^1
10^2
10^3
Current density (mA cm^{-2})